B20-type FeGe on Ge(100) prepared by pulsed laser melting

Li, Z.; Xie, Y.; Yuan, Y.; Wang, M.; Xu, C.; Hübner, R.; Prucnal, S.; Zhou, S.;

Originally published:

March 2021

Journal of Magnetism and Magnetic Materials 532(2021), 167981

DOI: https://doi.org/10.1016/j.jmmm.2021.167981

*B*20-type FeGe on Ge(100) prepared by pulsed laser melting

Z. Li[1,2*], Y. Xie[1,2], Y. Yuan[1,3], M. Wang[1], C. Xu[1], R. Hübner[1], S. Prucnal[1], S. Zhou[1*]

[1]Helmholtz-Zentrum Dresden-Rossendorf, Institute of Ion Beam Physics and Materials Research, Bautzner Landstrasse 400, D-01328 Dresden, Germany

[2]Technische Universität Dresden, D-01062 Dresden, Germany

[3] Songshan Lake Materials Laboratory, Dongguan, Guangdong 523808, People's Republic of China

* Corresponding author: Zichao Li and Shengqiang Zhou

E-mail address: zichao.li@hzdr.de & s.zhou@hzdr.de

Abstract: *B*20-type FeGe is one of the noncentrosymmetric materials hosting magnetic skymions. In this work, we have prepared *B*20-type FeGe films by pulsed laser melting of metal Fe deposited on Ge(100). The formation of the *B*20 phase is confirmed by X-ray diffraction. The FeGe samples show a superparamagnetic behaviour and their blocking temperatures increase with increasing the pulsed laser energy density. We conclude that this phenomenon is due to the increased grain size of the *B*20-type FeGe with increasing laser energy density. The presented method can be used to obtain different *B*20-type transition metal germanides and silicides, which can be magnetic skyrmion-hosting materials for spintronics.

Keyword: *B*20 phase, FeGe, Pulsed laser melting, Superparamagnetism

Introduction

There are two main ways of storing digital information for computing applications: solid-state random access memories (RAMs) and magnetic hard disk drives (HDDs) [1, 2]. Although the low cost of HDDs is very attractive, these devices are intrinsically slow and consume more electrical power than RAM. To improve the performance of the magnetic storage devices, one alternative approach is the construction of racetrack memory, which uses a train of magnetic domains separated by domain walls (DWs) in magnetic materials to code the information [3]. To read or write the information, the train of DWs can be moved electrically by spin torque [4]. However, before this approach can be used in practical applications, challenges such as reducing the critical current for moving the DWs must be addressed [5]. The intrinsic properties of magnetic skyrmions makes them competitive to solve some of these challenges [6, 7].

The creation/ annihilation of skyrmions by spin-polarized currents demonstrates a method of writing/deleting information in high speed [8, 9]. Magnetic skyrmions are nanoscale spin configurations originating from chiral interactions, known as Dzyaloshinskii–Moriya interactions (DMIs) [10, 11]. As reported, *B*20-type transition-metal germanides or silicides such as FeGe, MnSi [12-14] can be carriers hosting skyrmions. The *B*20-type structure is non-centrosymmetric and hence lacks inversion symmetry, resulting in a DMI which tends to favour orthogonal spin configurations [15-17]. Up to now, the most prominent skyrmion phase in *B*20 materials can only be realized below room temperature and at finite magnetic fields [8, 18-22]. For practical applications, it is necessary to have a stable skyrmion phase at room temperature and wide magnetic field range. Thin films are a good avenue for achieving these goals, since the size effect can increase the range of temperatures and magnetic fields within which skyrmions are stable [8, 12, 13]. Among the reported *B*20-type materials, FeGe has the highest ordering temperature of 278 K, which brings skyrmions closer to practical applications [17, 21-23].

Up to now, most FeGe films have been synthesized by magnetron sputtering in ultrahigh vacuum [21-24]. In our work, we fabricated *B*20-type FeGe by depositing a Fe film on a Ge wafer followed by non-equilibrium Pulsed Laser Melting (PLM) [25]. PLM allows fast heating up of solid surfaces on a time scale of nanoseconds [26, 27]. It can reach remarkably high temperatures and only melt the sample surface, which imparts minimal thermal damage to the substrate. Furthermore, melting films can form new phases by liquid phase epitaxy in an ultra-fast non-equilibrium cooling process. The *B*20-type FeGe phase formation in our films was proved by X-ray diffraction (XRD) and transmission electron microscopy (TEM). Moreover, we found that the FeGe grain size can be tuned by changing the energy density of the laser.

Experimental

As the first step, a 10-nm-thick Fe film was deposited on a Ge(100) wafer through electron-beam evaporation. Afterwards PLM was used to melt the sample surface and recrystallize the melted layer. In this annealing process, the deposited samples were melted using a pulsed Xe-Cl excimer laser (Coherent COMPexpro201, wavelength of 308 nm, pulse duration of 20 ns) in ambient air [26]. The germanidation process was performed using a single laser pulse of beam size 5×5 mm^2 with the energy density varied from 0.2 to 0.8 J/cm^2.

To analyze the microstructure of the PLM-treated FeGe film, X-ray diffraction (XRD) and transmission electron microscopy (TEM) were employed. XRD was performed by a Bruker D8 Advance diffractometer with a Cu-target source. Bragg-Brentano-geometry with a graphite

secondary monochromator and a scintillation detector were used in this setup. Cross-sectional bright-field and high-resolution TEM imaging were performed using an image-Cs-corrected Titan 80-300 microscope (FEI) operated at an accelerating voltage of 300 kV. High-angle annular dark-field scanning transmission electron microscopy (HAADF-STEM) imaging and spectrum imaging analysis based on energy-dispersive X-ray spectroscopy (EDXS) were done at 200 kV with a Talos F200X microscope equipped with an X-FEG electron source and a Super-X EDX detector system (FEI).

The magnetic properties were studied by using a superconducting quantum interference device equipped with a vibrating sample magnetometer (SQUID-VSM) with the field parallel (in-plane) to the films. For the zero-field cooling (ZFC) measurements, the samples were cooled down to 5 K under a zero field, then the field was switched to 50, 200, or 500 Oe and magnetization data were collected during the warming up process. When reaching 350 K, the samples were re-cooled to 5 K at the same field while the data recording was continued (field cooling (FC) measurements). The transport properties of FeGe were investigated in a Lake Shore Hall measurement system. Magnetic-field-dependent resistance was measured at 5–300 K using van der Pauw geometry.

Results and discussion

The room-temperature XRD patterns of the PLM-treated samples are shown in Figure 1. The two diffraction peaks located at around 31.6^{o} and 66.0^{o} arise from the diffraction at the (200) and (400) planes of the Ge wafer. After annealing with a laser energy density of 0.2 J/cm^2, the top Fe layer was not molten and the XRD spectra is the same like in as-deposited sample, implying that this energy density is too low to melt the sample surface and form a new crystalline phase. As the laser energy density increases to at least 0.4 J/cm^2, two extra peaks around 32.7^{o} and 68.2^{o} become detectable. These new peaks originate from the diffraction at the (111) and (222) planes of *B*20-type FeGe [28]. Moreover, the FeGe film has a preferential orientation with the {111} planes parallel with the Ge (100) substrate surface [29].

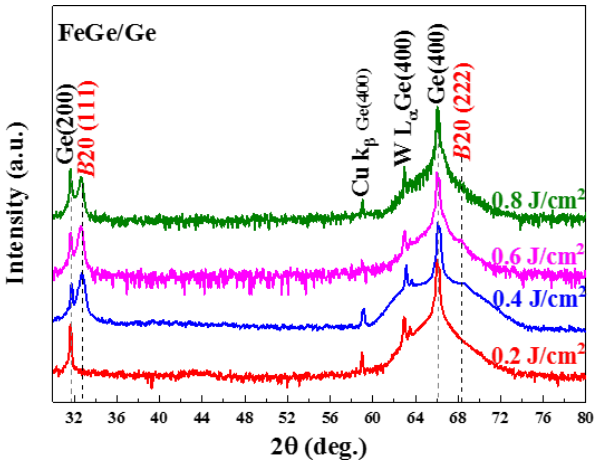

Figure 1 XRD patterns of the FeGe/Ge samples after PLM at various energy densities. With increasing energy density, the *B*20-type FeGe phase formation becomes obvious.

According to Bragg's law, $2d\sin\theta = n\lambda$, where λ is the wavelength of the incident X-rays ($\lambda_{CuK\alpha}$ = 1.54 Å), n is the diffraction order and θ is the diffraction angle, the (111) lattice spacing is calculated to be 2.73 Å. This value is comparable with that of fully relaxed FeGe (2.74 Å) [29]. The peaks at 59.2° and 63.2 ° result from the diffraction at the Ge (400) planes by Cu K_β and W L_α X-rays, respectively [30].

The average FeGe grain size can be calculated using the Scherrer formula: $D = (0.94 * \lambda) / (\beta * \cos\theta)$, where D is the average grain size and β is the full width at half maximum (FWHM) of the diffraction peak [31]. The FWHM and corresponding grain size for the various PLM-treated samples are shown in Table 1. With increasing the energy density from 0.4 J/cm^2 to 0.8 J/cm^2, the average FeGe grain size increases from 23 nm to 28 nm.

Table.1 FWHM and FeGe grain sizes of the PLM-treated samples.

	0.4 J/cm^2	**0.6 J/cm^2**	**0.8 J/cm^2**
FWHM (°)	0.36	0.33	0.29
Grain size (nm)	23	25	28

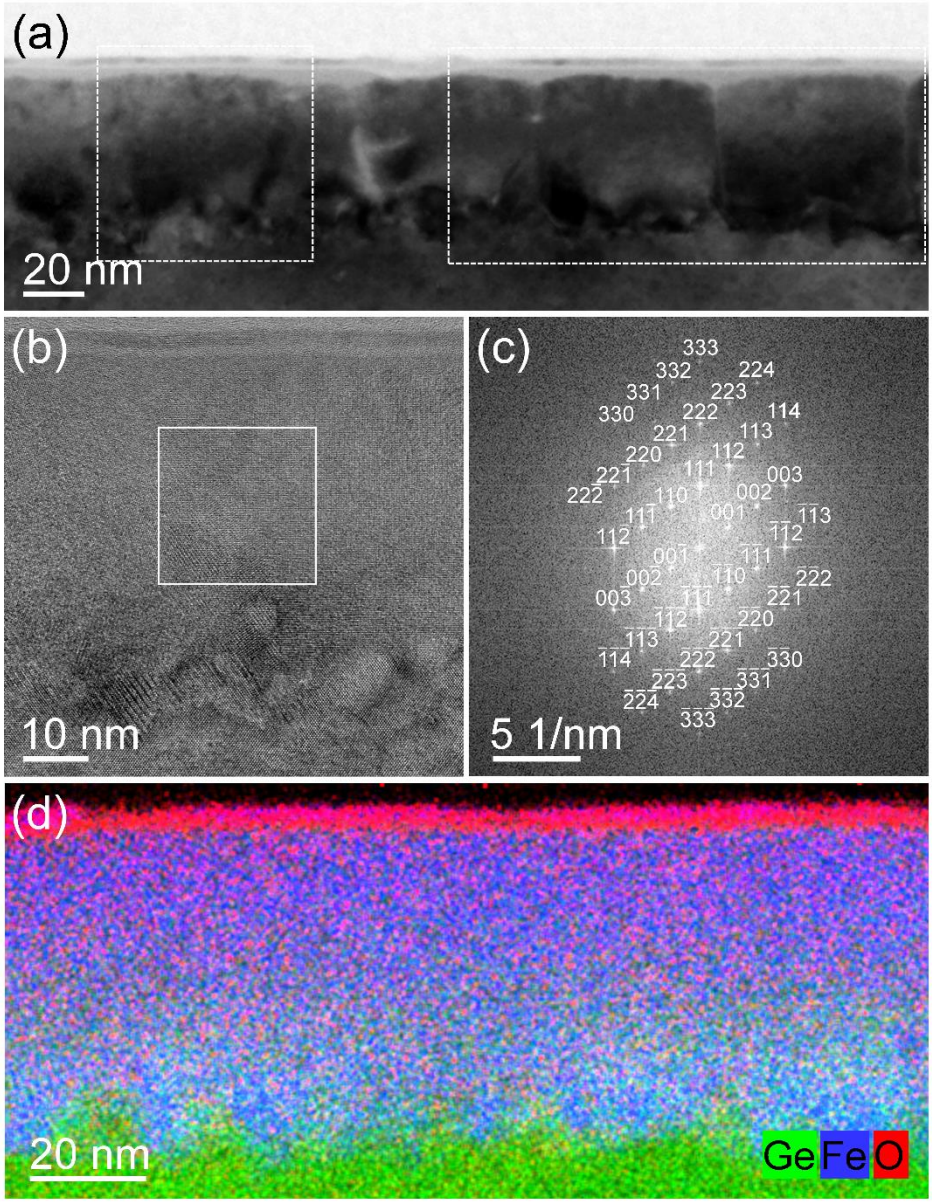

Figure 2 (a) Cross-sectional bright-field TEM image of the PLM-treated sample at 0.4 J/cm^2; (b) high-resolution image of the area marked with a dashed white square in panel (a); (c) fast Fourier transform of the region marked with a white square in panel (b) and indexed based on an FeGe [$\bar{1}$ 1 0] zone axis pattern; (d) superimposed EDXS-based element distributions (blue: iron, green: germanium, red: oxygen) for the area marked with a white dashed rectangle in panel (a).

A representative cross-sectional bright-field TEM image of the Fe/Ge sample annealed at an energy density of 0.4 J/cm^2 is shown in Figure 2(a). Below a 4-nm-thin surface film consisting of two single layers (see EDXS results), there is an about 55-nm-thick film which is mainly composed of equiaxed grains (dark-gray appearance with slightly varying orientation contrast) and only shows an up to 7-nm-thick amorphous contribution (light-grey with uniform brightness). To further characterize the phase structure of the crystalline part, high-resolution TEM imaging (Figure 2(b)) combined with fast Fourier transform analysis (Figure 2(c)) was performed. Taking the *B20*-type FeGe structure, the diffractogram in Figure 2(c) can be

described by a [$\bar{1}$ 1 0] zone axis pattern (in particular: normal to the growth plane [1 1 1] FeGe is parallel to [0 0 1] Ge and in-plane [$\bar{1}$ 1 0] FeGe is parallel to [$\bar{1}$ 1 0] Ge). This result is in good accordance to the XRD findings. The spatial distribution of the elements Fe, Ge, and O was characterized by EDXS-based analysis in scanning TEM mode and is shown in Figure 2(d). Although the lateral Fe distribution in the germanide layer is homogeneous, there is a dependence on depth. While the Fe:Ge atomic ratio directly below the sample surface is determined to be close to 1:1, the Fe content decreases with further depth due to limited diffusion of Fe into the Ge substrate during PLM treatment. Above the Fe germanide, there is an oxide layer composed of a Fe oxide on top of a Ge oxide, explaining the above-mentioned two-fold gradation of the surface layer. The small oxygen signal within the Fe germanide region is caused by TEM lamella side-wall oxidation during storage in air. For thicker TEM lamella positions, this O signal is even less pronounced.

The magnetization curves of the FeGe films synthesized at different PLM energy densities under an in-plane field recorded at various temperatures are shown in Figure 3. For each curve, the linear diamagnetic background of the Ge wafer was subtracted. It is clear that the PLM-treated FeGe films show a hysteresis behaviour at 5 K. The coercivity is 46, 20, and 39 mT for FeGe films annealed at a PLM energy density of 0.4 J/cm^2, 0.6 J/cm^2, and 0.8 J/cm^2, respectively. With increasing the energy density of the laser, the saturation magnetization increases, because higher annealing energy promotes the reaction between Fe and Ge (below the Curie temperature of the FeGe films [21]). However, above 100 K, the hysteresis behaviour disappears in the magnetization curves (see Figure 3(a)-(c)), indicating the superparamagnetic nature in the FeGe films [32].

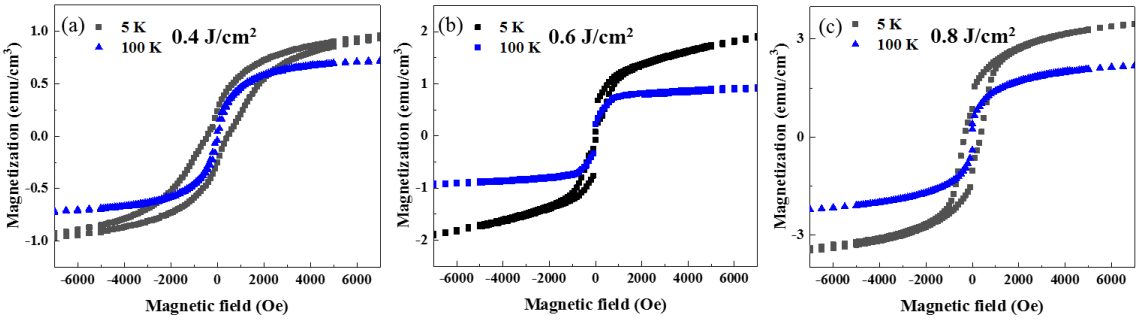

Figure 3 Magnetic hysteresis loops of the PLM-treated samples measured at different temperatures, (a) 0.4 J/cm^2; (b) 0.6 J/cm^2; (c) 0.8 J/cm^2. All these samples show ferromagnetic hysteresis at 5 K, while the hysteresis disappears at 100 K.

Figure 4(a)-(c) shows the ZFC/FC magnetization curves measured at different fields for the FeGe films. The ZFC/FC magnetization curves show an irreversibility, originating from the anisotropy barrier which blocks the magnetization orientation in the nanoparticles cooled under

zero field [33]. At low temperature, the randomly oriented magnetization of the nanoparticles is blocked in their initial states. At 5 K when the magnetic field is applied, some smaller nanoparticles with smaller magnetic anisotropy energy flip along the field direction. With increasing temperature, the thermal activation energy increases and the magnetic field will flip the larger particles. This process results in the increase of the magnetization in the ZFC curve with temperature. The peak of the ZFC curves, T_b, is considered as the blocking temperature of the sample. Above the blocking temperature, the ZFC magnetization decreases with temperature due to the increase of thermal fluctuations.

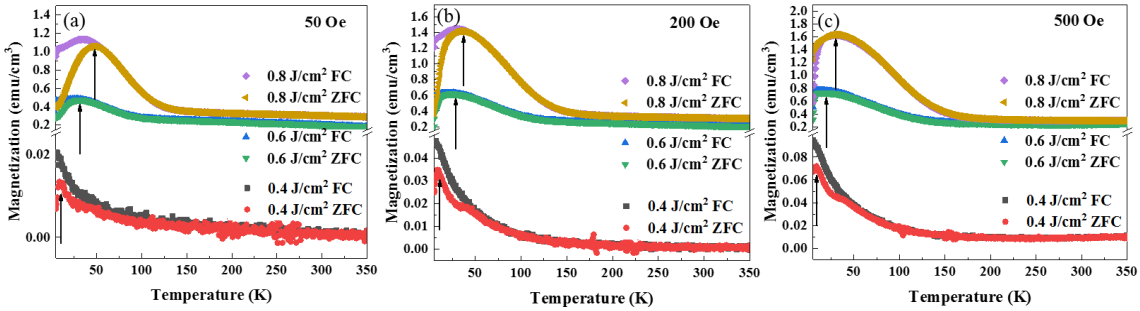

Figure 4 Zero-field cooling and field cooling magnetization curves for the PLM-treated samples measured under (a) 50 Oe, (b) 200 Oe and (c) 500 Oe. With increasing the energy density, the blocking temperatures (T_b, indicated by the arrows) shifts to higher temperature due to an increase of the grain size. With increasing the applied field, the blocking temperatures move to lower temperature.

At the same applied field, for example at 50 Oe, the blocking temperatures are 8.5, 33, and 45 K for the FeGe film synthesized at PLM energy densities of 0.4, 0.6, and 0.8 J/cm^2, respectively. It is obvious that T_b moves to higher temperature with increasing the laser energy density. As expected, T_b shows the same trend at 200 and 500 Oe. It is reported that the blocking temperature of $MgFe_2O_4$ spinel ferrite nanoparticles increases with increasing particle size [34]. As indicated by the XRD results, a higher intensity of the laser pulse can promote the growth of larger grains. Therefore, we conclude that the increasing grain size of FeGe films with increasing the PLM energy density moves T_b to higher temperatures. For each sample at different applied field, T_b decreases when the field is increased. The blocking temperatures are summarized in Table 2.

Table 2 Blocking temperatures of samples depending on the energy density during PLM treatment and the applied magnetic field.

	0.4 J/cm^2	**0.6 J/cm^2**	**0.8 J/cm^2**
T_b at 50 Oe (K)	8.5	33	45
T_b at 200 Oe (K)	8.1	27	35

T_b at 500 Oe (K)	7.5	20	31

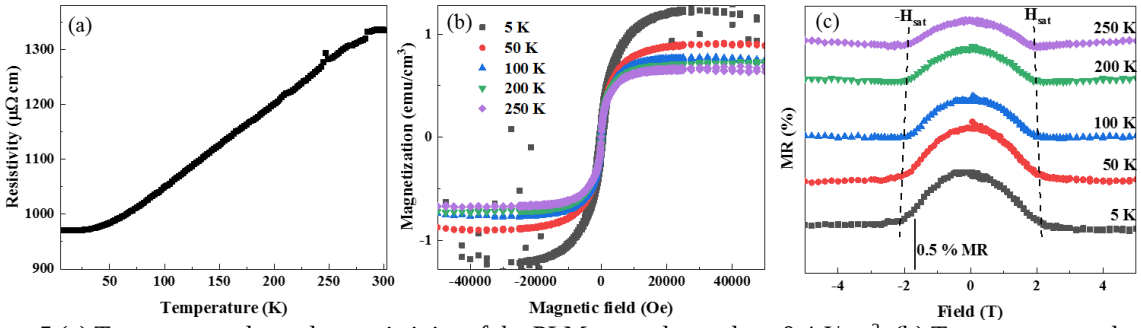

Figure 5 (a) Temperature-dependent resistivity of the PLM-treated sample at 0.4 J/cm^2; (b) Temperature evolution of the magnetization, measured under an out-of-plane field; (c) Magnetoresistance at various temperatures of the PLM-treated sample at 0.4 J/cm^2.

The temperature-dependent resistivity of the FeGe film treated by PLM at an energy density of 0.4 J/cm^2 is shown in Figure 5(a). It has the same shape as for previously reported FeGe films [21, 22]. At 5 K, the film characterized by a residual resistivity of around 960 μΩcm which is only slightly higher than the reported value for FeGe of 500 μΩcm [22]. With increasing temperature from 50 to 280 K, the resistivity exhibits roughly a linear characteristic which is typical for metal-like films [35]. The temperature evolution of the out-of-plane magnetization for the FeGe film treated at 0.4 J/cm^2 is shown in Figure 5(b). Different from the in-plane magnetization shown in Figure 3, there is no clear hysteresis resolved in the out-of-plane magnetization, in agreement to the results reported in Ref. 36. The saturation field H_{sat} is weakly temperature-dependent and is reduced from 2.25 T at 5 K to 1.9 T at 250 K.

Figure 5(c) shows the magnetoresistance (MR) at different temperatures under the out-of-plane magnetic field for the FeGe film treated at 0.4 J/cm^2. The MR is defined as $MR = \frac{R_{H-R_0}}{R_0} \times 100\%$, where R_H is the resistance under the magnetic field H and R_0 is the resistance without magnetic field. The shape of the MR curves also mimic the results shown in Ref. 36 for epitaxial FeGe films. At the field below the saturation (H_{sat}), the sample is suggested in a single conical magnetic phase [36], magnifying itself as the nearly linear dependence of M (magnetization) on the field (Figure 5(b)) and the conventional negative MR proportional to M^2 (Figure 5(c)) when the field is below H_{sat}. In Ref. 36, the smooth dependence of M and MR on the magnetic field is attributed to the possible continuous evolution of the cone angle. The similar MR behaviour in our FeGe samples also indicates the similar magnetic phase as in Ref. 36. The crystalline quality of our samples can be further optimized by varying the thickness of the Fe metal layer, the orientation of the Ge substrate and the PLM parameters.

Conclusions

In summary, *B*20-type FeGe was obtained by a simple method: room-temperature deposition of a Fe film on a Ge(100) substrate followed by pulsed laser melting. With increasing the laser energy density above 0.4 J/cm^2, FeGe grains preferentially <111>-oriented parallel to the Ge substrate normal form. With increasing the laser energy density, the average grain size increases causing higher blocking temperatures. Below the blocking temperature, the synthesized FeGe film shows ferromagnetic properties, while above the blocking temperature, the FeGe film shows superparamagnetism. Negative magnetoresistance is also observed, exhibiting a similar field dependence as epitaxial FeGe films. The presented thin film preparation method can be used to fabricate different skyrmions-hosting matrixes based on transition metal germanides and silicides.

Acknowledgments

The authors thank Andrea Scholz for her assistance in XRD measurements, Romy Aniol for TEM specimen preparation, and Bernd Scheumann for the deposition of Fe films. The author Z. Li (File No. 201707040077) acknowledges the financial support by the China Scholarship Council. Furthermore, the use of the HZDR Ion Beam Center TEM facilities and the funding of TEM Talos by the German Federal Ministry of Education of Research (BMBF), Grant No. 03SF0451, in the framework of HEMCP are acknowledged.

Reference

[1] J. G. Zhu, Mater. Today. 2003, 6, 22.

[2] I. R. McFadyen, E. E. Fullerton, M. J. Carey, MRS. Bull. 2006, 31, 379.

[3] S.S.P. Parkin, M. Hayashi, L. Thomas, Science. 2008, 320, 190.

[4] K. Ryu, L. Thomas, S. Yang, and S. Parkin, Nat.Nanotechnol. 2013, 8, 527.

[5] K. Shibata, X. Z. Yu, T. Hara, D. Morikawa, N. Kanazawa, K. Kimoto, S. Ishiwata, Y. Matsui, Y. Tokura, Nat. Nanotech. 2013, 8, 723.

[6] F. Jonietz, S. Muehlbauer, C. Pfleiderer, A. Neubauer, W.Muenzer, A. Bauer, T. Adams, R. Georgii, P. Boeni, R. A.Duine, K. Everschor, M. Garst, A. Rosch, Science 2010, 330, 1648.

[7] X. Z. Yu, N. Kanazawa, W. Z. Zhang, T. Nagai, T. Hara, K.Kimoto, Y. Matsui, Y. Onose, Y. Tokura, Nat. Commun. 2012, 3, 988.

[8] N. Nagaosa, Y. Tokura, Nat. Nanotech.2013, 8, 899.

[9] Y. Liu, N. Lei, C. Wang, X. Zhang, W. Kang, D. Zhu, Y. Zhou,X. Liu, Y. Zhang, W. Zhao, Phys. Rev. Appl. 2019 11, 014004.

[10] T. Moriya, Phys. Rev.1960, 120, 91.

[11] I. Dzyaloshinsky, J. Phys. Chem. Solids. 1958, 4, 241.

[12] Y. Li, N. Kanazawa, X. Z. Yu, A. Tsukazaki, M. Kawasaki, M. Ichikawa, X. F. Jin, F. Kagawa, Y. Tokura, Phys.Rev. Lett. 2013, 110, 117202.

[13] S. L. Zhang, I. Stasinopoulos, T. Lancaster, F. Xiao, A. Bauer, F. Rucker, A. A. Baker, A. I. Figueroa, Z. Salman, F. L. Pratt,S. J. Blundell, T. Prokscha, A. Suter, J. Waizner, M. Garst, D.Grundler, G. van der Laan, C. Pfleiderer, T. Hesjedal, Sci. Rep. 2017 7,123.

[14] N. Kanazawa, S. Seki, Y. Tokura, Adv. Mater. 2017, 29, 1603227.

[15] B. Binz, A. Vishwanath, and V. Aji, Phys. Rev. Lett. 2006 96, 207202.

[16] M. Bornemann, S. Grytsiuk, P. F. Baumeister, M. dos S. Dias, R. Zeller, S. Lounis, S. Blügel, J. Phys. Condens. Matter.2019 31, 485801.

[17] X. Z. Yu, Y. Onose, N. Kanazawa, J. H. Park, J. H. Han, Y. Matsui, N. Nagaosa, Y. Tokura, Nature, 2010, 465, 901.

[18] T. Schulz, R. Ritz, A. Bauer, M. Halder, M. Wagner, C.Franz, C. Pfleiderer, K. Everschor, M. Garst, A.Rosch, Nat. Phys. 2012, 8, 301.

[19] S. V. Grigoriev, V. A. Dyadkin, E. V. Moskvin, D. Lamago, T. Wolf, H. Eckerlebe, S. V. Maleyev, Phys. Rev. B. 2009, 79, 144417.

[20] S. V. Grigoriev, V. A. Dyadkin, D. Menzel, J. Schoenes, Y. O. Chetverikov, A. I. Okorokov, H. Eckerlebe, S. V. Maleyev, Phys. Rev. B. 2007, 76, 224424.

[21] S. X. Huang, C. L. Chien, Phys. Rev. Lett. 2012, 108, 267201.

[22] N. A. Porter, J. C. Gartside, C. H. Marrows, Phys. Rev. B. 2014, 90, 024403.

[23] X. Z. Yu, Y. Onose, N. Kanazawa, J. H. Park, J. H. Han, Y. Matsui, N. Nagaosa, Y. Tokura, Nat. Mater. 2011, 10, 106.

[24] J. C. Gallagher, K. Y. Meng, J. T. Brangham, H. L. Wang, B. D. Esser, D. W. McComb, F. Y. Yang, Phys. Rev. Lett. 2017, 118, 027201.

[25] Y. Yuan, R. Hübner, M. Birowska, C. Xu, M. Wang, S. Prucnal,R. Jakiela, K. Potzger, R. Böttger, S. Facsko, J. A. Majewski, M.Helm, M. Sawicki, S. Zhou, T. Dietl, Phys. Rev. Materials. 2018, 2, 114601.

[26] M. Wang, Y. Berencén, E. García-Hemme, S. Prucnal,R. Hübner, Y. Yuan, C. Xu, L. Rebohle, R. Böttger, R.Heller, H. Schneider, W. Skorupa, M. Helm, S. Zhou, Phys. Rev. Appl. 2018, 10, 024054.

[27] M. Lonsky, J. Teschabai-Oglu, K. Pierz, S. Sievers, H. W.Schumacher, Y. Yuan, R. Böttger, S. Zhou, J. Müller, Phys. Rev. B. 2018, 97, 054413.

[28] International Centre for Diffraction Data Powder Diffraction File card 04-019-1088.

[29] W. Y. Wu, W. W. Tjiu, W. Wan, H. R. Tan, S. L. Teo, S. Guo, S. T. Limc, M. Lin, Cryst. Eng. Comm. 2018, 20, 2916.

[30] Y. Xie, Y. Yuan, M. Wang, C. Xu, R. Hübner, J. Grenzer, Y. Zeng, M. Helm, S. Zhou, S. Prucnal, Appl. Phys. Lett. 2018, 113, 222401.

[31] A. L. Patterson, Phys. Rev. 1939, 56, 978-981.

[32] L.D. Tung, V. Kolesnichenko, G. Caruntu, D. Caruntu, Phys. B. 2002, 319, 116–121.

[33] A. Kundu, C. Upadhyay, H. C. Verma, Phys. Lett. A, 2003, 311, 410–415.

[34] Chen. Qi, Z. John, Appl. Phys. Lett. 1998, 73, 21.

[35] E. Ertekin, M. T. Winkler, D. Recht, A. J. Said, M. J. Aziz, T. Buonassisi, J. C. Grossman, Phys. Rev. Lett. 2012, 108, 026401.

[36] N. Kanazawa, J. S. White, H. M. Rønnow, C. D. Dewhurst,Y. Fujishiro, A. Tsukazaki, Y. Kozuka, M. Kawasaki, M.Ichikawa, F. Kagawa, Y. Tokura, Phys. Rev. B. 2016, 94, 184432.